Surface & Coatings Technology 409 (2021) 126885

Contents lists available at ScienceDirect

Surface & Coatings Technology

journal homepage: www.elsevier.com/locate/surfcoat

Wear and corrosion resistant coatings prepared on LY12 aluminum alloy by plasma electrolytic oxidation

Chao Yang [a], Jiayu Zhu [a], Suihan Cui [a], Pinghu Chen [a], Zhongcan Wu [a], Zhengyong Ma [a], Ricky K. Y. Fu [b], Xiubo Tian [a], Paul K. Chu [b], Zhongzhen Wu [a,*]

[a] School of Advanced Materials, Peking University Shenzhen Graduate School, Shenzhen 518055, China
[b] Department of Physics, Department of Materials Science & Engineering, Department of Biomedical Engineering, City University of Hong Kong, Tat Chee Avenue, Kowloon, Hong Kong, China

ARTICLE INFO

Keywords:
Plasma electrolytic oxidation (PEO)
Aluminum alloy
Wear resistance
Corrosion resistance

ABSTRACT

Although aluminum alloys are widely used in the aerospace industry, their relatively poor wear and corrosion resistance have hampered some applications and reduce the lifetime of the components. In this work, by using a zinc-containing phosphate electrolyte, the corrosion resistance, surface hardness, and wear resistance of the coatings produced by plasma electrolytic oxidation (PEO) are simultaneously improved. The micro-arc discharge is optimized by changing the phosphate concentration instead of introducing hard phase cations to improve the crystallinity of the zinc-doped alumina coating. Our results reveal that by using a concentration of $(NaPO_3)_6$ of 50 g/L, the hard phase of crystralline alumina and corrosive-resistant phase of $Zn_3(PO_4)_2$ are produced in concert. In the salt spraying test, the lifetime of the PEO coating is over 5000 h and the electrochemical corrosion current density is reduced by about 2 orders of magnitude confirming the improved corrosion resistance and durability. Moreover, the surface hardness increases from 400 HV for the coating prepared using the conventional phosphate electrolyte to 711.8 HV and the wear rate also drops from 8.5×10^{-4} $mm^3 \cdot (N \cdot m)^{-1}$ to 2.0×10^{-5} $mm^3 \cdot (N \cdot m)^{-1}$. This strategy can guarantee the aluminum alloy PEO coating with simultaneous excellent wear and corrosion resistance to cope with the complex service environment.

1. Introduction

Aluminum and aluminum alloys are commonly used in the aerospace and other industry because of the light weight, high strength, and easy molding [1–4]. However, as the chemical activity of aluminum alloys is relatively high, they corrode easily in media with high salt contents such as seawater [5]. In addition to the poor corrosion resistance, industrial machineries and components made of aluminum alloys show unacceptable wear and tear in long-term use. In this respect, deposition of a surface coating can strengthen valve metals such as aluminum alloys [6–8] and plasma electrolytic oxidation (PEO) boasts advantages such as process simplicity and economy, environmental friendliness, and ability to process components with a complex geometry [9,10]. In the PEO process, the micro-arc discharge triggered in the electrolyte forms a molten surface on which the electrolyte reacts with the substrate to produce a thick oxide coating. However, owing to the energetic liquid plasma discharge, the oxide coating which is usually rough and microporous has relatively poor corrosion resistance, resulting in a 600–800 h neutral salt spray time [11]. Generally, by introducing nanoparticles or salts containing Mo, Ca, Ti, Fe and so on into the electrolyte, insoluble or poorly soluble compounds can be created in the coating to form a physical barrier to improve the corrosion resistance so that the salt spray time can extend to 1000–2000 h [12–15]. Our previous work produced an insoluble zinc phosphate layer on the PEO coating to achieve super-hydrophilicity and self-healing of the pores and the materials could withstand salt spraying for 11,000 h [16]. However, incorporation of the anti-corrosion phase reduces the mechanical properties and wear resistance of the coating, resulting in a reduced life once the coating is mechanically damaged. Typically, some elements such as Zr, W, and Mn have been incorporated into the electrolyte to form hard oxide to improve the hardness of the coatings [17–19]. At the same time, lubricating phases of MoS_2, graphene, graphite particles, $CePO_4$, and other two-dimensional materials have been incorporated to reduce the friction coefficient [20–22]. Generally, introduction of hard phases or lubricating phases tend to reduce the corrosion resistance due to the competitive cations in the electrolyte. Besides, complex

* Corresponding author.
E-mail address: wuzz@pkusz.edu.cn (Z. Wu).

https://doi.org/10.1016/j.surfcoat.2021.126885
Received 30 August 2020; Received in revised form 14 December 2020; Accepted 8 January 2021
Available online 17 January 2021

electrolytes containing multiple elements may cause agglomeration or precipitation and subsequently unstable discharges in PEO. A feasible solution is to optimize the concentration and hydrolysis of the main salts in the electrolyte to improve the crystallinity of the alumina coatings without introducing additional hard phases [23,24].

In this work, by using an electrolyte containing Zn, the arc discharge intensity and scale are controlled to improve the crystallinity of the alumina coating and consequently both the corrosion resistance as well as wear resistance. Incorporation of the functional zinc phosphate in the coating guarantee the lifetime of neutral salt spray above 5000 h. a larger salt concentration enhances the arc discharge intensity and arc splashing and greatly improves the hardness of the coating. The coating prepared under the optimal conditions are demonstrated to have excellent corrosion resistance and wear resistance.

2. Experiments section

2.1. Materials

The commercial aluminum alloy (LY12, 50 mm × 25 mm × 1 mm) purchased from Shenzhen Xinhongyun Hardware Mould Co., Ltd. (Shenzhen, China) was the substrate and analytical grade acetone, absolute ethanol, and zinc acetate ($Zn(AC)_2$) were purchased from Sinopharm Chemical Reagent Co., Ltd. (Shanghai, China). The other chemical reagents including sodium hexametaphosphate ($(NaPO_3)_6$) and sodium ethylenediaminetetraacetate (EDTA-2Na) were analytical grade and obtained from Guangdong Xilong Chemical Co., Ltd. (Shantou, China). All the reagents were used without purification.

2.2. Coating preparation

The LY12 alloy was ultrasonically cleaned with ethanol and acetone for 5 min and dried in air. A 20 kW AC bipolar power supply (Plasma Technology Ltd., China) was employed in PEO and the electrolyte contained 30 g/L $Zn(AC)_2$, 10 g/L EDTA-2Na and 10–60 g/L $(NaPO_3)_6$. The current density was 10 A/dm^2, duty cycle was 12%, frequency was 750 Hz, and processing time was 12 min. An external water cooling system was used to ensure that the temperature of the electrolyte was below 55 °C during PEO.

2.3. Sample characterization

The surface and cross-sectional morphologies of the PEO coatings were observed on a field-emission scanning electron microscope (FE-SEM, Carl Zeiss, SUPRA®55), and the elemental distribution and composition of the coatings were determined by energy-dispersive X-ray spectroscopy (EDS). The phase composition and crystallinity were determined by X-ray diffraction (XRD) with a Cu source ($\lambda = 0.15418$ nm) at $2\theta = 10°$–$80°$ and scanning rate of $2\theta = 5°$ min^{-1} with a 0.01 step size. The X-ray photoelectron spectroscopy (XPS, ESCALAB 250×, Thermo Fisher) spectra were referenced to the C1s peak (284.8 eV) and the coating thickness was determined by an eddy current thickness meter (CTY2300, SDCH. Co.; LTD). The surface roughness was assessed using a surface roughness tester (JD220, JitaiKeyi, China). A Vicker hardness tester (HV-1000, Shanghai Jvjing, China) was employed to measure the hardness of the coatings under a load of 0.3 N and a 3D confocal microscope (VK X200, KEYENCE) was used to monitor the corrosion process and examine the wear tracks.

2.4. Corrosion and wear tests

The corrosion characteristics were determined by electrochemical and salt spraying tests. The former was carried out on an electrochemical workstation (1470E, Solartron Metrology) to obtain the polarization curves at a scanning rate of 3 mV/s and 25 °C with platinum as the counter electrode and the saturated calomel electrode as the reference electrode. The sample with a surface area of 3.14 cm^2 was exposed to the 3.5 wt% NaCl solution. The Tafel data were collected and the corrosion potential (E_{corr}) and corrosion current density (i_{corr}) were derived by extrapolation. The salt spraying test was performed using the ASTM B117 protocol on a salt spray tester (SN-60A, Sannuo Instrument Co., Ltd., China). The sodium chloride concentration was 5 wt% and the pH was 6.5–7.0.

The wear test was carried out on a ball-on-disk machine (MFT-5000, Rtec instruments, USA) at ambient temperature (humidity <30%) against a silicon nitride ball with a diameter of 4 mm. The load was 4 N, rotation speed was 100 r/min, rotation diameter was 5 mm, and time was 180 min. The wear rate W (mm^3·(N·m)$^{-1}$) was calculated by the following equation [25]:

$$W = V/(F \times 60\, t \times 2\pi nr), \quad (1)$$

where V (mm^3) is the wear volume, F (N) is the load force, t (s) is the time, n (m/s) is the speed, and r (m) is the radius of rotation. Five areas were measured and averaged to improve the statistics.

3. Results and discussion

3.1. Materials characterization

Fig. 1 shows the voltage versus time curves during the PEO process. Generally, the voltage increases gradually with time because the resistance of the coating increases as a result of the insulating oxide for a constant current density. In the first stage (0–1 min), the voltage increases rapidly to 350 V and a passivation layer is generated on the aluminum alloy. The anions from the electrolyte accumulate on the passivation layer to produce channels at the weakest point and then react with the molten metal to form the oxide coating [26,27]. In the second stage (1–10 min), the rate of coating generation decreases as the oxide layer becomes thicker. In the last stage (10–12 min), the oxide layer becomes thick enough to facilitate a stable discharge and the voltage is maintained at about 550 V [28]. If the concentration of $(NaPO_3)_6$ is increased, the slope of the voltage-time curve decreases gradually and the end voltage becomes smaller. This is because incorporation of phosphate increases the conductivity of the electrolyte and reduces the relative resistance of the electrolyte, resulting in a decline of the actual power consumption.

Fig. 2 shows the surface morphology of the coatings revealing that the surface becomes heterogeneous after PEO. Under the high temperature and high pressure discharge condition, the molten materials splash out, cool, shrink, and finally solidify to produce crater-like porous structures together with flat structures with a certain size and density on the surface, suggesting melting around the pores [26]. The surface morphology of the coatings prepared in electrolytes with different phosphate concentrations is different. As the concentration of phosphate

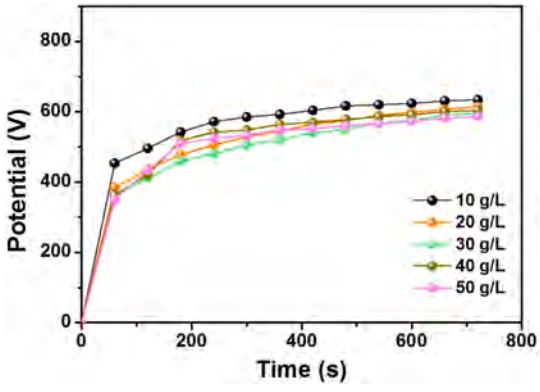

Fig. 1. Voltage-time curves of the coatings prepared electrolytes containing different concentrations of $(NaPO_3)_6$.

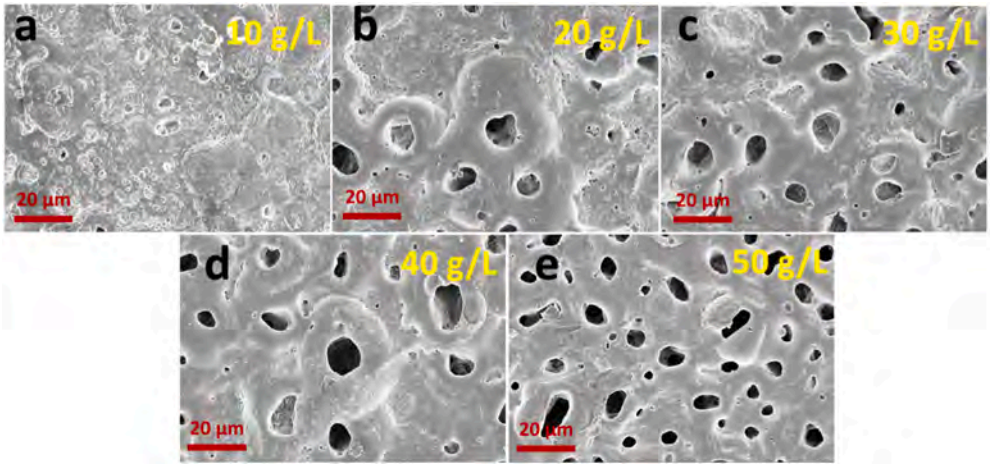

Fig. 2. SEM of the samples prepared with electrolytes containing different concentrations of $(NaPO_3)_6$: (a) 10 g/L, (b) 20 g/L, (c) 30 g/L (d) 40 g/L, (d) 50 g/L.

is increased from 10 g/L to 20 g/L, the structure shows more pores and the size increases from 5 μm to 18 μm (Fig. 2a and b). The reason is that more phosphate ions are clustered in the coatings to generate more discharge centers on the surface and therefore, a large amount of molten materials splash out to increase the pore size [10]. However, if the phosphate concentration is increased further, the pores size does not change and even decreases but the density increases, indicating that the arc becomes denser (Fig. 2c to e). Owing to the denser and more uniform discharge, the growth rate of the coatings is accelerated and the surface roughness decreases as shown in Table 1. The Zn concentration in the coating slightly decreases with increasing phosphate concentration because Zn is incorporated into the coatings during arc retraction which weakens gradually with increasing arc energy, as shown in Table 2. As a result, the Zn concentration decreases to 6.09 at.% when the phosphate concentration is 50 g/L.

The XPS results in Fig. 3 show the presence of Al, Zn, C, O and P confirming that Zn and P are embedded into the coating consistent with EDS. Carbon may arise from atmospheric contaminants. The P 2p peak at 133.7 eV corresponds to $[PO4]^{3-}$ [29,30] (Fig. 3b) and the Zn 2p peaks at 1022.2 eV and 1045 eV are associated with Zn $2p_{3/2}$ and Zn $2p_{1/2}$ in $Zn_3(PO_4)_2$ [31] (Fig. 3c). The O 1s spectrum of the coating prepared with the 50 g/L phosphate solution can be divided into two peaks, P-O-Zn at 532.6 eV and Al—O at 532 eV [27,32] suggesting that $Zn_3(PO_4)_2$ (doped phase) and Al_2O_3 (main phase) are present in the coatings.

Fig. 4 presents the XRD results of the coatings prepared with electrolytes containing different phosphate concentrations. The background peak and overlapping peak between 20° and 35° reveal a large amount of amorphous component in the coatings. The diffraction peak at 21.5° corresponds to the crystalline phase of $Zn_3(PO_4)_2$ [32] corroborating doping of $Zn_3(PO_4)_2$. The peak at 45.8° is from the (400) plane of γ-Al_2O_3 which is the main crystalline phase in the coatings determining the hardness [33]. The inset in Fig. 4 shows the diffraction angles from 45.5° to 46.5° and the intensity of γ-Al_2O_3 (400) increases with phosphate concentrations reaching the maximum at 50 g/L. The diffraction peaks from α-Al_2O_3 at 37.2° and 43.1° indicate better crystallinity of the

Table 1
Thickness and roughness of the samples prepared with electrolytes containing different concentrations of $(NaPO_3)_6$.

Concentration of $(NaPO_3)_6$ (g/L)	Thickness (μm)	Surface roughness (Ra , μm)
10	30 ± 1	1.89 ± 0.05
20	34 ± 1	1.85 ± 0.05
30	36 ± 1	1.63 ± 0.05
40	35 ± 1	1.62 ± 0.09
50	36 ± 1	1.47 ± 0.06

Table 2
EDS results of the samples prepared with electrolytes containing different concentrations of $(NaPO_3)_6$.

Concentration of $(NaPO_3)_6$ (g/L)	Atom percentage(%)			
	O	Al	Zn	P
10	64.76	18.79	9.82	6.26
20	68.3	14.62	9.28	7.87
30	68.24	14.88	8.63	7.79
40	64.85	19.75	7.73	7.65
50	69.89	16.12	6.09	7.43

Al_2O_3 in coatings as the phosphate concentration is increased because at a higher concentration, more charges are created on the surface to increase the reaction energy. Fig. 5 shows the hardness of the coatings prepared with electrolytes containing different phosphate concentrations. As the phosphate concentration goes up, the hardness increase linearly from 412.6 HV for 10 g/L to 711.8 HV for 50 g/L due to the better crystallinity [34,35].

3.2. Corrosion resistance

Fig. 6 displays the electrode polarization curves of the PEO and untreated samples and Table 3 lists the corrosion potentials (E_{corr}) and corrosion current densities (i_{corr}) derived by extrapolation. The corrosion potentials of PEO samples increase from −1.451 V to −1.046 V, whereas the corrosion current densities decrease by two orders of magnitude from 1.758×10^{-5} A/cm^2 to 1.275×10^{-7} A/cm^2. The results indicate that incorporation of zinc phosphate into the coatings obstruct the traffic between the corrosive solution and coatings. The corrosion potentials decrease from −1.406 V for 10 g/L to −1.073 V for 50 g/L. On the contrary, the corrosion current densities increase from 1.275×10^{-7} A/cm^2 to 2.045×10^{-7} A/cm^2 because of the relative increase of alumina and decrease of zinc phosphate in the coatings with increasing phosphate concentrations. Furthermore, the large number of pores create more channels to aggravate corrosion [36]. Nevertheless, the electrochemical corrosion effect is much better than that of the untreated and conventional PEO samples.

After salt spraying for 5000 h, there are no changes in the morphology and no obvious corrosion spots on the surface (Fig. 7a). For confirmation, no corrosion pits or corrosion products are observed by 3D confocal microscopy (200 X) demonstrating excellent corrosion resistance even though the Zn concentration decreases when the phosphate concentration goes up (Fig. 7b). The micro-morphology after salt spraying for 5000 h are presented in Fig. 8a which disclose no corrosion pits and corrosion cracks. But a sponge-like lamella structures in some

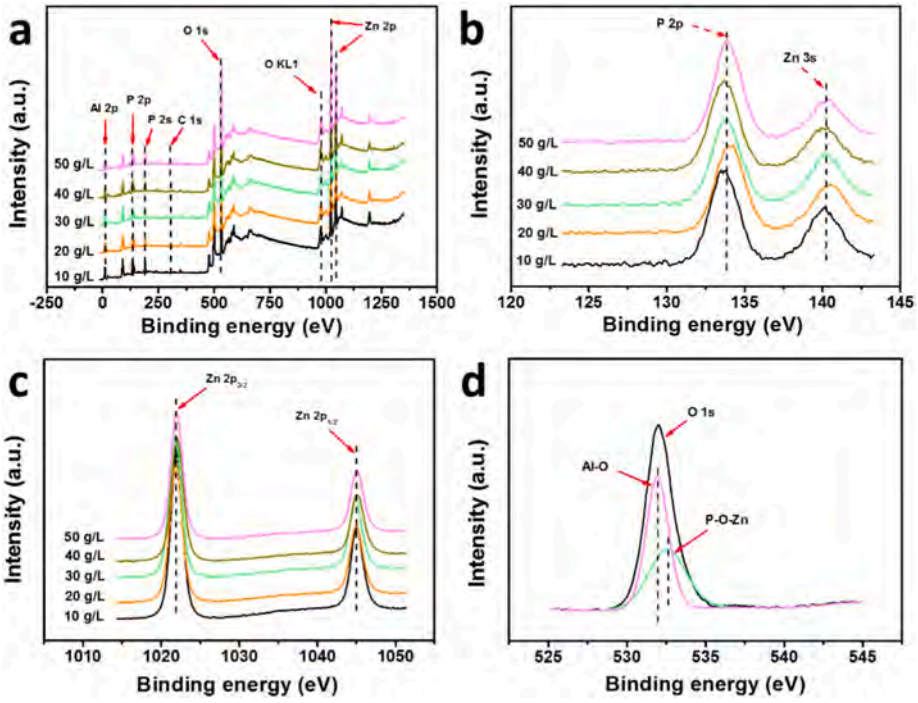

Fig. 3. XPS results of the coatings prepared with electrolytes containing different concentrations of $(NaPO_3)_6$: (a) Survey spectra, (b) P 2p and Zn 3 s spectra, (c) Zn 2p3/2 and Zn 2p1/2 spectra; (d) O 1 s spectrum of the coating prepared with the 50 g/L phosphate solution.

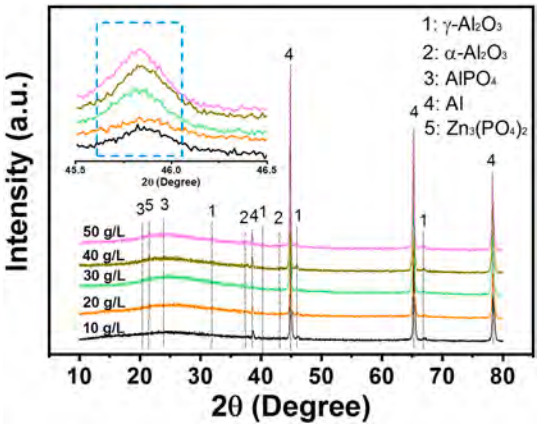

Fig. 4. XRD spectra of the coatings prepared with electrolytes containing different concentrations of $(NaPO_3)_6$.

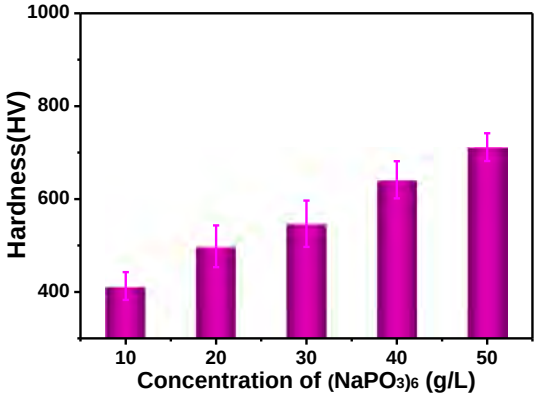

Fig. 5. Microhardness of the coatings prepared with electrolytes containing different concentrations of $(NaPO_3)_6$.

pores indicative of slight local corrosion (Fig. 8b) [37]. The cross-sectional morphology discloses that the pore wall is relatively smooth and solid without visible corrosion (Fig. 8c). EDS performed on the cross-section of the hole shows that O, Al, and P are uniformly distributed but Zn is concentrated in the hole and on the surface (Fig. 8d). The corrosion lifetime of 5000 h in neutral salt spray indicates that the coating embedded in zinc phosphate has excellent corrosion resistance and can satisfy requirements for most corrosive environments.

3.3. Wear resistance

Fig. 9a shows the friction coefficients of the coatings prepared with electrolytes containing different phosphate concentrations. In the initial stage (6–10 min), the friction coefficients increase gradually and abrasive particles are produced because of the rough porous structure. Subsequently, the abrasive particles create a relatively smooth protective film on the surface leading to a stable friction coefficient of about

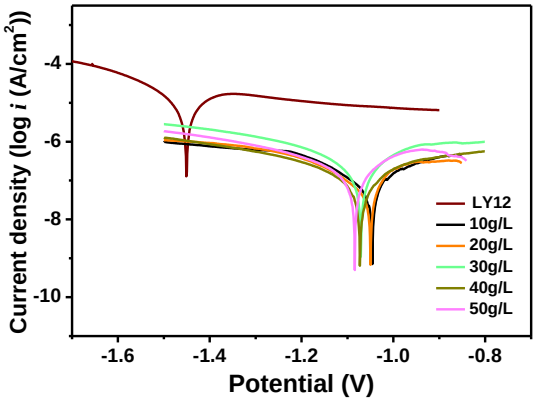

Fig. 6. Potential polarization curves of untreated LY12 and coatings prepared with electrolytes containing different concentrations of $(NaPO_3)_6$.

Table 3
Corrosion current densities and corrosion potentials of the untreated LY12 and PEO coatings prepared with electrolytes containing different concentrations of $(NaPO_3)_6$.

Samples	Current densities (A/cm^2)	Potentials (V)
LY12	1.758×10^{-5}	−1.451
10 g/L $(NaPO_3)_6$	1.275×10^{-7}	−1.046
20 g/L $(NaPO_3)_6$	1.862×10^{-7}	−1.054
30 g/L $(NaPO_3)_6$	1.936×10^{-7}	−1.071
40 g/L $(NaPO_3)_6$	1.962×10^{-7}	−1.084
50 g/L $(NaPO_3)_6$	2.045×10^{-7}	−1.073

0.7 [38]. However, the samples prepared with electrolytes containing phosphate concentrations of 10, 20, and 30 g/L are worn at time points of 75, 90, and 110 min, respectively. As a result, the friction coefficient decreases to around 0.4 after 15–20 min showing irreversible failure. In comparison, the friction coefficient of the coatings prepared with electrolytes containing larger phosphate concentrations (40 and 50 g/L) is stable at about 0.7 even after 180 min indicating much stronger protection. As the phosphate concentration is increased from 10 g/L to 50 g/L, the wear rates diminish from 8.5×10^{-4} $mm^3 \cdot (N \cdot m)^{-1}$ to 2.0×10^{-5} $mm^3 \cdot (N \cdot m)^{-1}$, as shown in Fig. 9b. The reduction is almost two orders of magnitude and the PEO coating prepared with a phosphate concentration of 50 g/L shows the best wear resistance, which is also a

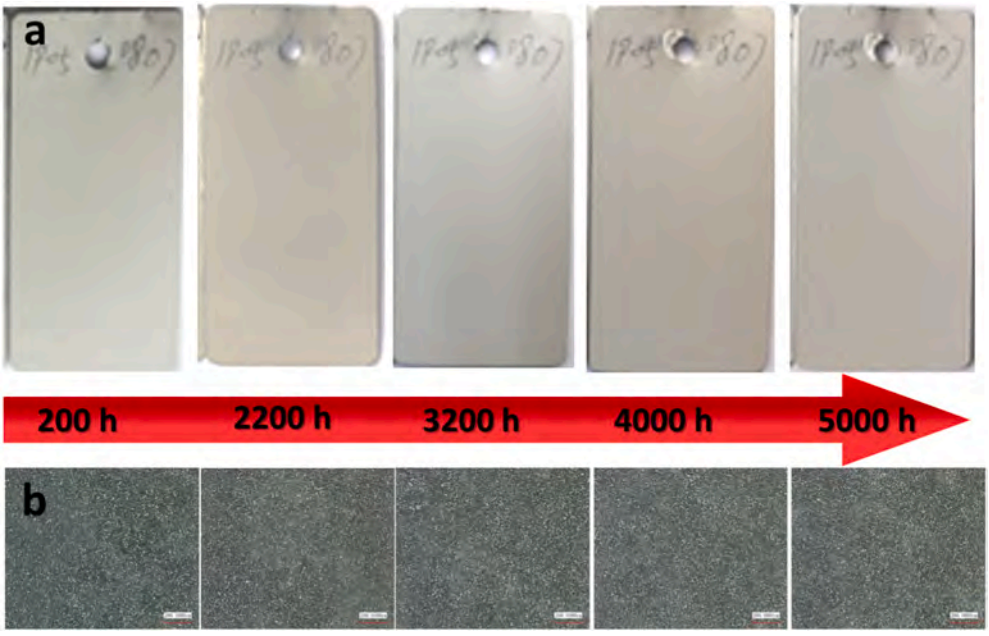

Fig. 7. (a) Optical photo, (b) 3D confocal image after salt spraying for different time of the sample prepared with the electrolyte containing 50 g/L $(NaPO_3)_6$.

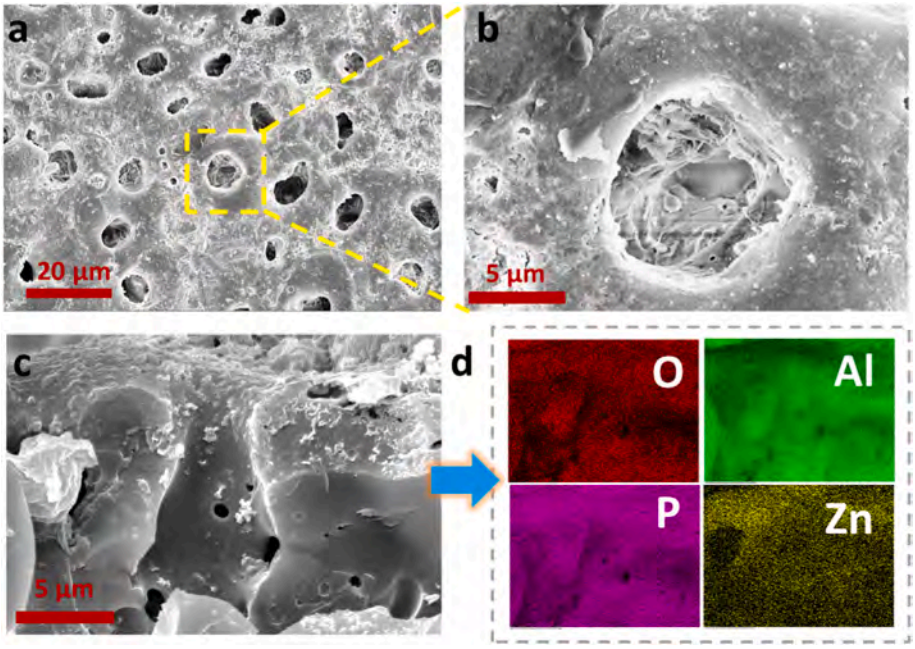

Fig. 8. SEM image (a and b), cross-sectional SEM images (c) and EDS maps (d) after salt spraying for 5000 h of the sample prepared with the electrolyte containing 50 g/L $(NaPO_3)_6$.

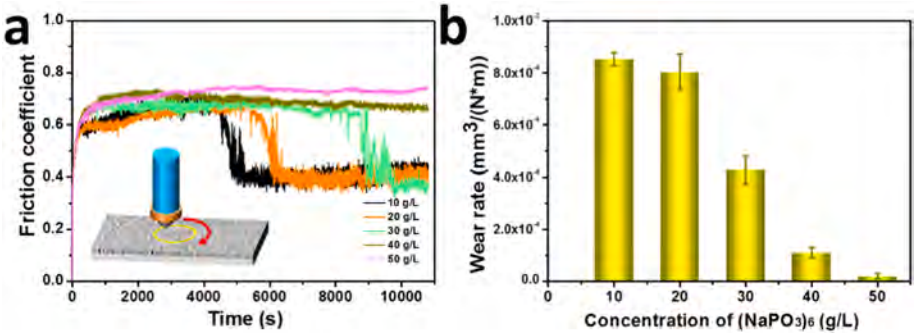

Fig. 9. (a) Friction coefficients and (b) Wear rates of the coatings prepared with electrolytes containing different concentrations of $(NaPO_3)_6$.

high level of the wear resistance in the conventional PEO coating prepared by phosphate system electrolyte [39–41].

Fig. 10 compares the wear images, optical photos of the wear tracks, and 3D morphology of coatings prepared with electrolytes containing different phosphate concentrations. The deep cracks and exposed substrates of the 10, 20, and 30 g/L samples reveal coatings failure. However, the shallower wear tracks of the 40 and 50 g/L samples indicate better wear resistance (Fig. 10a). The 3D images of the three former show track widths of more than 1 mm which is larger the coating thickness indicating that the coatings are worn (Fig. 10b). When the phosphate concentration is increased to 40 g/L, the width (0.6 mm) and depth of the wear track decrease evidently and the typical abrasive wear stems from that because of the relatively rough surface, the abraded particles fill the gaps [23]. When the phosphate concentration is further increased to 50 g/L, the crack is wider but depth is shallower. This is because the bottom of the silicon nitride ball was worn by the hard γ-Al_2O_3 phase in the coatings during the wear test [25]. The results show that the coating prepared with a phosphate concentration of 50 g/L exhibits stable wear resistance and long-term corrosion resistance, which can greatly extend the actual service life for most aluminum alloy components in engineering.

4. Conclusion

The crystallinity of the wear resistant phase of γ-Al_2O_3 is improved by increasing the phosphate concentration in the electrolyte in PEO and the stable and optimized discharge conditions produce coatings with excellent wear resistance and corrosion resistance. The salt spraying test reveals a lifetime of more than 5000 h even though the zinc phosphate concentration in the coatings decreases as the phosphate concentration in the electrolyte goes up. Compared to the untreated LY12 aluminum alloy, the corrosion current density of the PEO coating is about two orders of magnitude smaller and the corrosion potential increases from −1.451 V to −1.046 V confirming remarkable corrosion protection. A larger phosphate concentration in the electrolyte enhances the crystallinity of the hard Al_2O_3 phase and the coating prepared with a phosphate concentration of 50 g/L shows a hardness of 711.8 HV and wear rate of 2.0×10^{-5} $mm^3 \cdot (N \cdot m)^{-1}$. By increasing the concentration in the

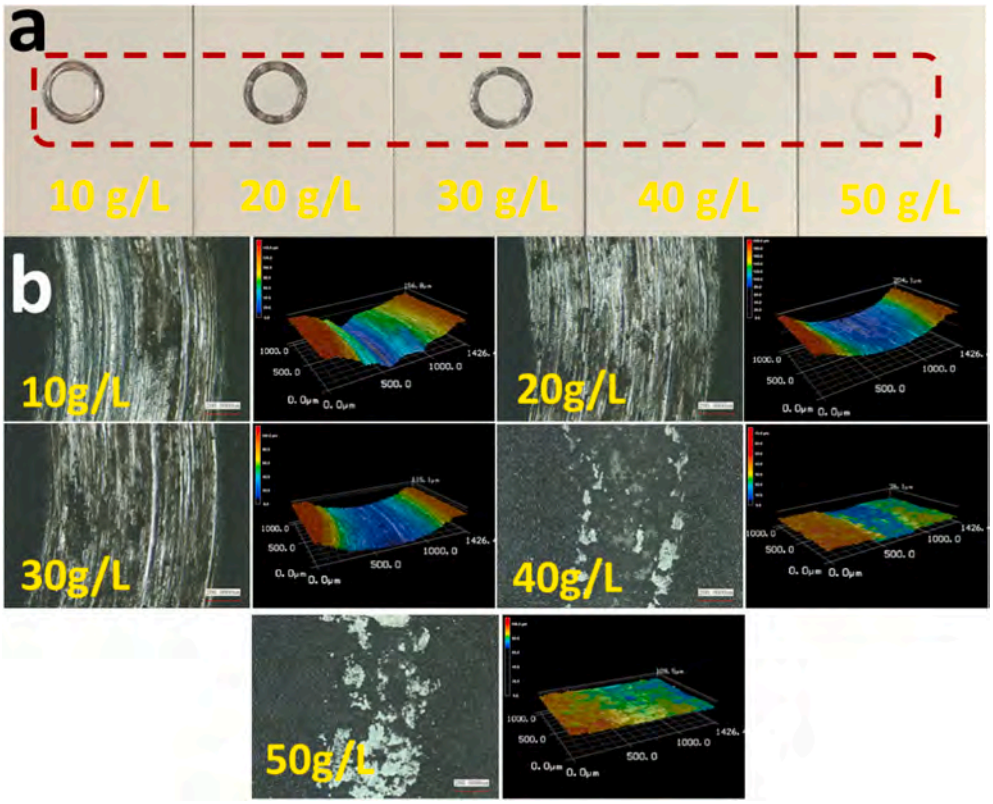

Fig. 10. (a) Wear tracks, (b) 3D confocal photos of the wear tracks on the coatings prepared with electrolytes containing different concentrations of $(NaPO_3)_6$.

electrolyte, decrease of corrosion-resistant phase content caused by cation competition can be avoided consequently improving the wear resistance while maintaining the corrosion resistance at the same time. The strategy has large commercial potential in improving the mechanical properties and corrosion resistance of aluminum alloys.

CRediT authorship contribution statement

Zhongzhen Wu, Chao Yang and Jiayu Zhu proposed the research; Jiayu Zhu, Suihan Cui, Pinghu Chen, and Zhongcan Wu designed the coating depositions; Chao Yang, Jiayu Zhu and Zhengyong Ma did the coating characterizations and properties testing; Zhongzhen Wu, Chao Yang, Ricky K. Y. Fu, Xiubo Tian and Paul K. Chu analyzed and discussed the data; Chao Yang, Jiayu Zhu, Zhongzhen Wu and Paul K. Chu wrote the paper; Xiubo Tian and Paul K. Chu polished the English writing; all authors provided feedback.

Declaration of competing interest

The authors declare that they have no known competing financial interests or personal relationships that could have appeared to influence the work reported in this paper.

Acknowledgements

C.Y. and J.Z. contributed equally to this work. The authors would like to acknowledge for the financial support provided by Guangdong Basic and Applied Basic Research Foundation (No. 2019A1515011858), Postdoctoral Innovative Talent Support Program (No. BX20190001), City University of Hong Kong Strategic Research Grant (SRG) No. 7005264, Guangdong - Hong Kong Technology Cooperation Funding Scheme (TCFS) No. GHP/085/18SZ, and Hong Kong Research Grants Council (RGC) General Research Funds (GRF) No. CityU 11205617.

References

[1] A. Alizadeh, M. Maleki, A. Abdollahi, Preparation of super-high strength nanostructured B4C reinforced Al-2Cu aluminum alloy matrix composites by mechanical milling and hot press method: microstructural, mechanical and tribological characterization, Adv. Powder Technol. 28 (2017) 3274–3287.
[2] W. Wang, Q. Pan, X. Wang, Y. Sun, L. Long, Z. Huang, Mechanical properties and microstructure evolution of ultra-high strength Al-Zn-Mg-Cu alloy processed by room temperature ECAP with post aging, Mat. Sci. Eng. A-Struct. 731 (2018) 195–208.
[3] R.K. Jayaraj, S. Malarvizhi, V. Balasubramanian, Optimizing the micro-arc oxidation (MAO) parameters to attain coatings with minimum porosity and maximum hardness on the friction stir welded AA6061 aluminium alloy welds, Def. Technol. 13 (2017) 111–117.
[4] H. Yu, M. Wang, Y. Jia, Z. Xiao, C. Chen, Q. Lei, Z. Li, W. Chen, H. Zhang, Y. Wang, High strength and large ductility in spray-deposited Al-Zn-Mg-Cu alloys, J. Alloy. Compd. 601 (2014) 120–125.
[5] K.M. Lee, Y.G. Ko, D.H. Shin, Incorporation of multi-walled carbon nanotubes into the oxide layer on a 7075 Al alloy coated by plasma electrolytic oxidation: coating structure and corrosion properties, Curr. Appl. Phys. 11 (2011) S55–S59.
[6] W. Xiaohong, Q. Wei, C. Bo, J. Zhaohua, L. Weiqiang, H. Weidong, White anodized thermal control coating on LY12 aluminum alloy, J. Mater. Process. Tech. 200 (2008) 405–409.
[7] M. Pellizzari, High temperature wear and friction behaviour of nitrided, PVD-duplex and CVD coated tool steel against 6082 Al alloy, Wear 271 (2011) 2089–2099.
[8] X.K. An, C. Yang, Z.Z. Wu, L.L. Liu, S.N. Li, L. Zhou, W. Tang, Z.Y. Ma, Z.C. Wu, R. K.Y. Fu, X.B. Tian, H. Lin, F. Pan, P.K. Chu, Self-regulated super-hydrophobic Cu/CuO electrode film deposited by one-step high-power sputtering, Adv. Electron. Mater. 1900891 (2019) 1–6.
[9] Y. Zhang, Y. Wu, D. Chen, R. Wang, D. Li, C. Guo, G. Jiang, D. Shen, S. Yu, P. Nash, Micro-structures and growth mechanisms of plasma electrolytic oxidation coatings on aluminium at different current densities, Surf. Coat. Tech. 321 (2017) 236–246.
[10] W. Li, Z. Qian, X. Liu, L. Zhu, H. Liu, Investigation of micro-arc oxidation coating growth patterns of aluminum alloy by two-step oxidation method, Appl. Surf. Sci. 356 (2015) 581–586.
[11] Q.Z. Chen, Z.Q. Jiang, S.G. Tang, W.B. Dong, Q. Tong, W.Z. Li, Influence of graphene particles on the micro-arc oxidation behaviors of 6063 aluminum alloy and the coating properties, Appl. Surf. Sci. 423 (2017) 939–950.
[12] O.L. Li, M. Tsunakawa, Y. Shimada, K. Nakamura, K. Nishinaka, T. Ishizaki, Corrosion resistance of composite oxide film prepared on Ca-added flame-resistant magnesium alloy AZCa612 by micro-arc oxidation, Corros. Sci. 125 (2016) 99–105.
[13] Ji Min, Kaseem Hoon, Ko Mosab, Gun Young, Corrosion behavior of Al-1wt% Mg-0.85wt%Si alloy coated by micro-arc-oxidation using TiO_2 and Na_2MoO_4 additives: role of current density, J. Alloy. Compd. 723 (2017) 448–455.
[14] K. Raeissi, M.A. Golozar, X. Lu, C. Blawert, M.L. Zheludkevich, The effect of pulse waveforms on surface morphology, composition and corrosion behavior of Al2O3 and Al_2O_3/TiO_2 nano-composite PEO coatings on 7075 aluminum alloy, Surf. Coat. Tech. 324 (2017) 208–221.
[15] S.P. Ji, Y.C. Weng, Z.Z. Wu, Z.Y. Ma, X.B. Tian, R.K.Y. Fu, H. Lin, G.S. Wu, P. K. Chu, F. Pan, J. Alloy. Compd. 710 (2017) 452–459.
[16] Q. Huang, L. Liu, Z. Wu, S. Ji, P.K. Chu, Corrosion-resistant plasma electrolytic oxidation coating modified by zinc phosphate and self-healing mechanism in the salt-spray environment, Surf. Coat. Tech. 384 (2020) 125321.
[17] F. Shamsi, M. Khorasanian, S.M. Lari Baghal, Effect of potassium permanganate on corrosion and wear properties of ceramic coatings manufactured on CP-aluminum by plasma electrolytic oxidation, Surf. Coat. Tech. 346 (2018) 63–72.
[18] A. Hakimizad, K. Raeissi, M. Santamaria, M. Asghari, Effects of pulse current mode on plasma electrolytic oxidation of 7075 Al in Na_2WO_4 containing solution: from unipolar to soft-sparking regime, Electrochim. Acta 284 (2018) 618–629.
[19] L. Zhang, W. Zhang, Y. Han, W. Tang, A nanoplate-like α-Al_2O_3 out-layered Al_2O_3-ZrO_2 coating fabricated by micro-arc oxidation for hip joint prosthesis, Appl. Surf. Sci. 361 (2016) 141–149.
[20] K.J. Ma, M.M.S. Al Bosta, W.T. Wu, Preparation of self-lubricating composite coatings through a micro-arc plasma oxidation with graphite in electrolyte solution, Surf. Coat. Tech. 259 (2014) 318–324.
[21] Q. Chen, Z. Jiang, S. Tang, W. Dong, Q. Tong, W. Li, Influence of graphene particles on the micro-arc oxidation behaviors of 6063 aluminum alloy and the coating properties, Appl. Surf. Sci. 423 (2017) 939–950.
[22] P. Chen, Z. Wu, Q. Huang, S. Ji, Y. Weng, Z. Wu, Z. Ma, X. Chen, M. Weng, R.K. Y. Fu, H. Lin, X. Tian, F. Pan, P.K. Chu, A quasi-2D material $CePO_4$ and the self-lubrication in micro-arc oxidized coatings on Al alloy, Tribol. Int. 138 (2019) 157–165.
[23] K. Zhang, S. Yu, Preparation of wear and corrosion resistant micro-arc oxidation coating on 7N01 aluminum alloy, Surf. Coat. Tech. 388 (2020) 125453.
[24] Y. Cheng, T. Wang, S. Li, Y. Cheng, J. Cao, H. Xie, The effects of anion deposition and negative pulse on the behaviours of plasma electrolytic oxidation (PEO)-a systematic study of the PEO of a Zirlo alloy in aluminate electrolytes, Electrochim. Acta 225 (2017) 47–68.
[25] Gecu Ridvan, Yakup, Emre Yurekturk, Faiz Tekoglu, Ahmet Muhaffel, Improving wear resistance of 304 stainless steel reinforced AA7075 aluminum matrix composite by micro-arc oxidation, Surf. Coat. Tech. 368 (2019) 15–24.
[26] J. Martin, A. Nominé, F. Brochard, J.L. Briançon, C. Noël, T. Belmonte, T. Czerwiec, G. Henrion, Delay in micro-discharges appearance during PEO of Al: evidence of a mechanism of charge accumulation at the electrolyte/oxide interface, Appl. Surf. Sci. 410 (2017) 29–41.
[27] G. Lv, W. Gu, H. Chen, W. Feng, M.L. Khosa, L. Li, E. Niu, G. Zhang, S.-Z. Yang, Characteristic of ceramic coatings on aluminum by plasma electrolytic oxidation in silicate and phosphate electrolyte, Appl. Surf. Sci. 253 (2006) 2947–2952.
[28] Z. Yao, Y. Jiang, F. Jia, Z. Jiang, F. Wang, Growth characteristics of plasma electrolytic oxidation ceramic coatings on Ti-6Al-4V alloy, Appl. Surf. Sci. 254 (2008) 4084–4091.
[29] E. Song, Y.-T. Kim, J. Choi, Anion additives in rapid breakdown anodization for nonmetal-doped TiO_2 nanotube powders, Electrochem. Commun. 109 (2019) 106610.
[30] F. Jamali-Sheini, K.R. Patil, D.S. Joag, M.A. More, Synthesis of Cu-ZnO and C-ZnO nanoneedle arrays on zinc foil by low temperature oxidation route: effect of buffer layers on growth, optical and field emission properties, Appl. Surf. Sci. 257 (2011) 8366–8372.
[31] H. Zeng, W.R. Lacefield, XPS, EDX and FTIR analysis of pulsed laser deposited calcium phosphate bioceramic coatings: the effects of various process parameters, Biomaterials 21 (2000) 23–30.
[32] R.K. Brow, An XPS study of oxygen bonding in zinc phosphate and zinc borophosphate glasses, J. Non-Cryst. Solids 194 (1996) 267–273.
[33] N. Xiang, X. Han, Y. Bai, Q. Li, J. Zheng, Y. Li, Y. Hou, Z. Huang, Size effect of γ-Al_2O_3 supports on the catalytic performance of Pd/γ-Al_2O_3 catalysts for HCHO oxidation, Mol. Catal. 494 (2020) 111112.
[34] Ghafaripoor Masoud, Raeissi Keyvan, Santamaria Monica, Hakimizad Amin, The corrosion and tribocorrosion resistance of PEO composite coatings containing α-Al_2O_3 particles on 7075 Al alloy, Surf. Coat. Tech. 349 (2018) 470–479.
[35] S. Wang, F. Guo, H. Bai, H. Yan, J. Liu, Microstructure and wear resistance of micro-arc oxidized ceramic coatings on Zr-4 alloy in different electrolyte systems, Rare. Metal. Mat. Eng. 39 (2010) 739–742.
[36] Z. Zhao, Q. Pan, J. Yan, J. Ye, Y. Liu, Direct current micro-arc oxidation coatings on Al-Zn-Mg-Mn-Zr extruded alloy with tunable structures and properties templated by discharge stages, Vacuum 150 (2018) 155–165.
[37] T.H. Nguyen, R.T. Foley, ChemInform abstract: the chemical nature of aluminum corrosion. III. The disssolution mechanism of aluminum oxide and aluminum powder in various electrolytes, Cheminform 12 (1981) 2563–2566.
[38] X.-J. Li, M. Zhang, S. Wen, X. Mao, W.-G. Huo, Y.-Y. Guo, Y.-X. Wang, Microstructure and wear resistance of micro-arc oxidation ceramic coatings prepared on 2A50 aluminum alloys, Surf. Coat. Tech. 394 (2020) 125853.
[39] B. Haghighat-Shishavan, R. Azari-Khosrowshahi, S. Haghighat-Shishavan, M. Nazarian-Samani, N. Parvini-Ahmadi, Improving wear and corrosion properties

of alumina coating on AA7075 aluminum by plasma electrolytic oxidation: effects of graphite absorption, Appl. Surf. Sci. 481 (2019) 108–119.
[40] Z.W. Li, S.C. Di, Preparation and properties of micro-arc oxidation self-lubricating composite coatings containing paraffin, J. Alloy. Compd. 719 (2017) 1–14.
[41] K. Zhang, S.R. Yu, Preparation of wear and corrosion resistant micro-arc oxidation coating on 7N01 aluminum alloy, Surf. Coat. Tech. 388 (2020) 125453.